ARTICLE

OPEN

Transverse optical pumping of spin states

Or Katz[1,2] & Ofer Firstenberg [1]

Optical pumping is an efficient method for initializing and maintaining atomic spin ensembles in a well-defined quantum spin state. Standard optical pumping methods orient the spins by transferring photonic angular momentum to spin polarization. Generally the spins are oriented along the propagation direction of the light due to selection rules of the dipole interaction. Here we present and experimentally demonstrate that by modulating the light polarization, angular momentum perpendicular to the optical axis can be transferred efficiently to cesium vapor. The transverse pumping scheme employs transversely oriented dark states, allowing for control of the trajectory of the spins on the Bloch sphere. This new mechanism is suitable and potentially beneficial for diverse applications, particularly in quantum metrology.

[1] Department of Physics of Complex Systems, Weizmann Institute of Science, 76100 Rehovot, Israel. [2] Rafael Ltd, IL-31021 Haifa, Israel. Correspondence and requests for materials should be addressed to O.K. (email: or.katz@weizmann.ac.il)

Optical pumping is the prevailing technique for orienting atomic spins, conveying order from polarized light onto the state of spins[1–3]. Many applications in precision metrology[4–7], quantum information[8–10], noble gas hyper-polarization[11–13], and searches for new physics beyond the standard model[14,15] employ optical pumping for initializing the orientation moment of the spins, that is, for pointing the spins towards a preferred direction. The required degree of polarization depends on the specific application, where optimized performance in quantum metrology is often practically achieved around 50% polarization[16–18]. Standard optical pumping schemes generate polarization along the propagation direction of the laser beam. These schemes include depopulation pumping[1], synchronous pumping[19–21], spin-exchange indirect pumping[22,23], alignment-to-orientation conversion[24,25], and hybrid spin-exchange pumping[16]. However, in various applications, it is often desired to polarize the spins along an applied magnetic field, perpendicular to the optical axis[18,26–30]. While at extreme magnetic fields, it is possible to polarize the spins transversely[31], at moderate magnetic fields, typical to alkali-metal spin experiments for example, the pumping efficiency is rather low.

In standard optical pumping schemes, the atomic ground state is polarized via repeated cycles of absorption and spontaneous emission. Ideally, the atoms cease to absorb the pump photons when they reach a 'dark state', which is determined by the excited transitions during pumping[1]. For a light field with an electric field $\mathbf{E}(t) = E_0 e^{i(\omega_L t - kx)}\hat{e}$, the relevant transitions depend on the relative detuning of the light frequency ω_L from the atomic transition frequency ω_0, on the external electric and magnetic fields, and on the selection rules of the dipole interaction for polarization $\hat{e}$. For alkali-metal vapors, the latter enables the pumping process of spin orientation at moderate magnetic fields, when the ground and excited magnetic sublevels $|m_g\rangle$, $|m_e\rangle$ within each hyperfine manifold F_g, F_e are optically unresolved.

In the absence of magnetic field and for constant polarization $\hat{e}$, one-photon absorption of light does not produce spin orientation transversely to the optical axis. Circular light polarization $\hat{e}_\pm = (\hat{y} \pm i\hat{z})/\sqrt{2}$ orients the spins along the optical axis $\pm\hat{x}$ via the allowed transitions $m_e = m_g \pm 1$; For $F_e \leq F_g$, the maximally

polarized state $|m_g = \pm F_g\rangle$ is dark. Linearly polarized light $\hat{e} = \hat{y}, \hat{z}$ generates spin alignment along $\hat{x} \times \hat{e}$ and zero net orientation with the selection rules $m_e = m_g$ when tuned to the transition $F_g \to F_e = F_g - 1$. This generates a quadrupole magnetic moment[1], leaving both $|m_g = F_g\rangle$ and $|m_g = -F_g\rangle$ dark. It thus seems that no orientation is built perpendicularly to the optical axis $\hat{x}$ for any light polarization. In the presence of a constant magnetic field, precession around it may orient the spins along the transverse direction, but this is never achieved with considerable orientation. Our scheme overcomes this limitation and allows for transverse optical pumping of the spins by temporally modulating the light polarization.

Here we propose and demonstrate an optical pumping scheme for efficient spin polarization transversely to the propagation direction of the laser beam. The scheme incorporates a polarization-modulated light beam, which steers the spins in helical-like trajectories on the Bloch sphere around and along a transverse magnetic field, while gradually increasing their polarization. The scheme exhibits sharp resonances, reaching maximum efficiency when the optical modulation is resonant with the Larmor precession of the spins. We develop a simple analytical model for analyzing the experimental results and discuss the applicability of the scheme for various applications.

Results

Experimental pumping of cesium spins. We employ the experimental setup shown schematically in Fig. 1a, containing cesium vapor at room temperature. The energy level for a $I = 1/2$ model is shown in 1b. Setting a constant magnetic field $B\hat{z}$ determines the quantization axis $\hat{z}$ and the Larmor frequency $\omega_B = gB$, where $g = 0.35(2\pi)$ MHz/G is the gyro-magnetic ratio for cesium. For the transverse pumping, we use a *pump* beam, whose frequency is tuned to the D_1 transition $F_g = 4 \to F_e = 3$ and whose polarization is modulated according to

$$\hat{e}(t) = \cos(\theta)\hat{z} + ie^{i\omega t}\sin(\theta)\hat{y}. \qquad (1)$$

Here, $\sin(\theta)$ is the modulation depth and ω is the modulation angular frequency. For the sake of analysis and presentation, we introduce two far-detuned monitor beams propagating along $\hat{x}$ and $\hat{y}$, measuring the three-dimensional orientation state of the spins ($2S_x$, $2S_y$, $2S_z$) on the Bloch sphere during the pumping process. See Methods for additional experimental details.

In Fig. 2a–d, we present measurement and theoretical calculation of the spin dynamics on the Bloch sphere. Figure 2a shows a typical measurement of the pumping process during continuous pumping operation. We observe that the spin orientation follows a helical trajectory transversely to the optical axis $\hat{x}$. In this experiment, the pump power is $P_0 = 250\,\mu$W and the modulation frequency is tuned to resonate with the Larmor frequency $\omega_B \approx \omega = 1.5\,(2\pi)$ kHz. The final value of $2S_z$ quantifies the pumping efficiency. Its dependence on the modulation parameters ω and θ is shown in Fig. 3. We identify two resonant features of $2S_z(\omega)$ at $\omega \approx \pm\omega_B$ as shown in Fig. 3a for $\theta = 0.24$ and two laser powers. The laser power governs the width of the resonance, as well as, the shift of the peak from the actual Larmor frequency. Figure 3b presents $2S_z(\theta)$ on one of the resonances [$\omega = 10.3\,(2\pi)$ kHz]. We achieved an overall maximal polarization of $2S_z = 65\%$ (with small residual transverse polarization $2\sqrt{S_x^2 + S_y^2} = 3.5\%$) as shown in Fig. 3c.

Dynamics of pumped spins. To explain the transverse pumping mechanism we utilize a simple model of an alkali-like level structure with nuclear spin $I = 1/2$, as shown in Fig. 1b. The magnetic field $\mathbf{B} = B\hat{z}$ (henceforth, assume $B > 0$) breaks the isotropy in the transverse yz plane, setting our quantization axis $\hat{z}$
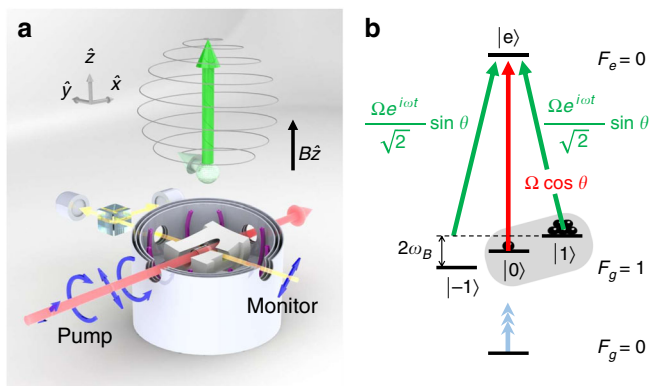

Fig. 1 Experimental system and toy model. **a** Schematics of the experimental setup and the spiral motion of the atomic spins (green) towards $+\hat{z}$. The polarization of the pump beam (red) alternates between linear and circular (blue arrows). The spin orientation is monitored using balanced polarimetry of a far-detuned monitor beam (yellow). Not shown are the repump beam and a second monitor beam, which co-propagate with the pump. **b** Toy model for alkali atoms with nuclear spin $I = 1/2$. The repump laser (blue arrow) empties the lower hyperfine state (with quantum number $F_g = 0$), while the pump laser (red and green arrows) drives the atoms into the dark state $|d_+\rangle \propto \cos\theta|1\rangle - \frac{1}{\sqrt{2}}e^{i\omega t}\sin\theta|0\rangle$ (gray shading), eventually oriented perpendicular to the beam direction
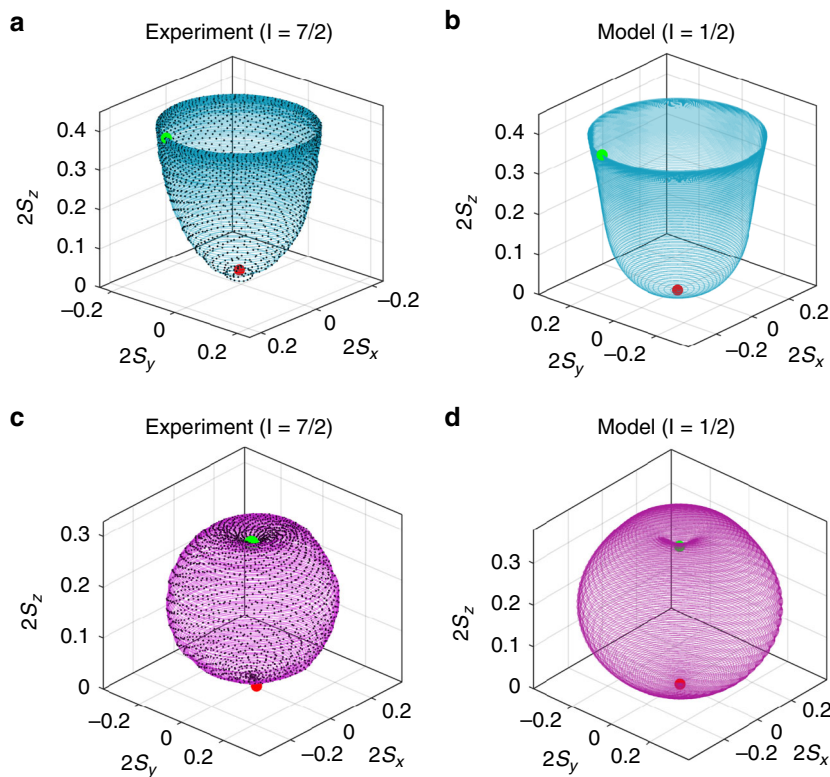
Fig. 2 Spin trajectories on the Bloch sphere. The optical axis is $\hat{x}$, within the equatorial plane. **a**, **c** Measurements of the pumping process from $t = 0$ to $t = 100$ ms. **b**, **d** Theoretical toy model with nuclear spins $I = 1/2$. Red (green) circles mark the initial (final) states of the spin. **a** When pumping with a constant modulation depth $\theta = 0.2$ rad, the measured cesium spins follow a spiral-helical trajectory around the $+\hat{z}$ direction. **c** Adiabatically varying $\theta(t) = \arccos\sqrt{t/T}$ over $T = 100$ ms allows for driving the spins in a spherical-helical trajectory that ends along the $\hat{z}$ axis
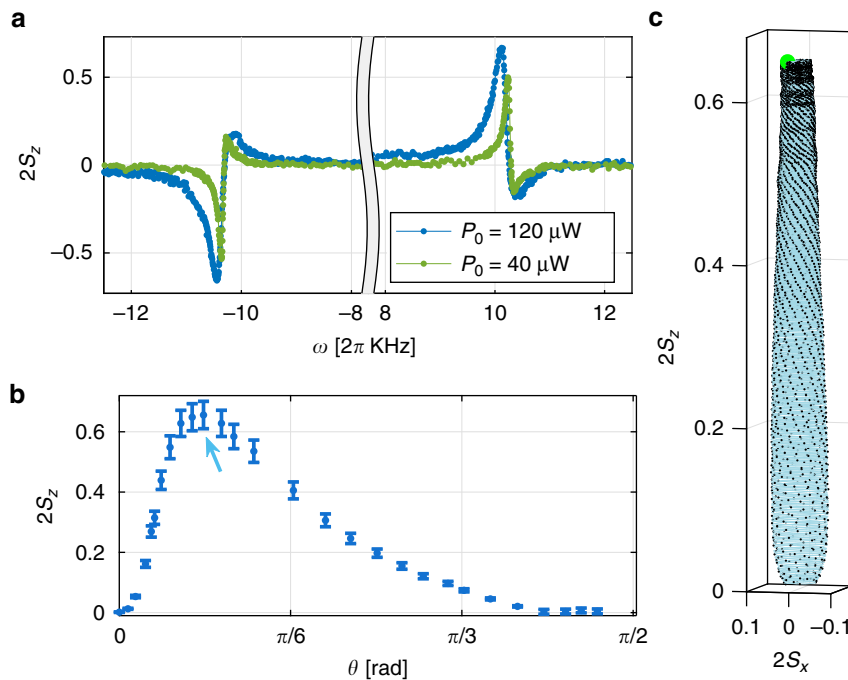

Fig. 3 Dependence of the pumping degree on the modulation parameters. **a** Measured spin $S_z(\omega)$ at $t = 200$ ms for cesium atoms with a modulation depth $\theta = 0.24$ rad and Larmor precession rate $\omega_B = 10.2$ (2π) kHz. The resonance peaks at modulation frequency $\omega \approx \pm \omega_B$ are associated with the two coherent population trapping (CPT) dark states $|d_\pm\rangle$. **b** Dependence on the modulation depth θ: measured $S_z(\theta)$ at $t = 200$ ms with $\omega = \pm 10.3$ (2π) kHz and pump power $P_O = 120$ μW. Pumping is optimal at moderate modulation depths, such that $|d_+\rangle$ is oriented towards $+\hat{z}$, but the dark state pumping $\Gamma \sin^2(\theta)$ competes the relaxation rate γ. Vertical error bars indicate standard deviation of the measured value. **c** Measured spin trajectory, corresponding to the point marked by an arrow in **b**. The final polarization (green circle) is along $\hat{z}$, i.e. perpendicular to the optical axis, with a small residual polarization along $\hat{x}$ and $\hat{y}$

and splitting the Zeeman sublevels $|0\rangle, |\pm 1\rangle$ by $\hbar\omega_B$. The $F_g = 0$ level is emptied by a repump field or by spin–exchange collisions. The pump field, resonant with the $F_g = 1 \rightarrow F_e = 0$ transition, is polarization-modulated according to Eq. (1). We describe the effect of the polarization modulation on the spin dynamics by decomposing the polarization vector $\hat{e}(t)$ into its Stokes components $\hat{s} = (s_1, s_2, s_3)$[32,33]. The unmodulated linear polarization $\hat{z}$, represented by s_1, aligns the atoms along $\hat{z}$ at a rate $R_a \sim \Gamma \cos^2(\theta)$, creating spin alignment (see Supplementary Note 1). Here $\Gamma = \Omega^2 / \gamma_e$ is the characteristic pumping rate, with γ_e the spontaneous emission rate and Ω the Rabi frequency of the pump beam. The linear polarization $(\hat{y} \pm \hat{z})/\sqrt{2}$, represented by s_2, induces a tensor light shift of $\Gamma \sin(2\theta) \sin(\omega t)$ along $\pm\hat{x}$, which acts like a magnetic field. This light shift appears when the linearly polarized light is neither parallel nor perpendicular to the spin alignment[34]. The circular polarization $\hat{e}_\pm$, represented by s_3, pumps the spins longitudinally along $\pm\hat{x}$ at a rate $\Gamma \sin(2\theta) \cos(\omega t)$, while vector light shift is absent for the resonant optical transition. Therefore, the modulated polarization alternates between pumping (s_3) and light shifting (s_2) the atomic spins along $\hat{x}$ at a rate ω. For $\omega = \omega_B$, the pumping and light shifts are synchronous, efficiently driving the precessing spins away from the xy plane, transversely to the optical axis. The resulting evolution of the Bloch vector $(2S_x, 2S_y, 2S_z)$ is shown graphically in Fig. 4 and further detailed in Methods.

The toy model enables one to reconstruct the main features of the measured trajectories as shown in Fig. 2b, by solving the $I = 1/2$ model numerically and tuning its parameters (see Supplementary Note 1). We note however that this model only aims at explaining the qualitative features of the process, while disregarding effects arising from the multilevel structure of cesium and from level mixing due to line broadening, which would reduce the pumping efficiency. We attribute these effects to the observed maximum of 65% polarization, rather than the 100% polarization expected for an $I = 1/2$ system (see Methods).

Coherent population trapping. The resonant nature of the pumping process can also be understood using the following supplementary picture, as originating from coherent population trapping (CPT)[35]. In CPT, a dark state is formed within a Λ level-system via destructive interference of two excitation pathways. Considering the level structure in Fig. 1b and decomposing the modulated pump into its two polarization components $E\hat{z}$ and $E\hat{y}$, we identify two Λ systems: $\Lambda_+ = \{|1\rangle, |e\rangle, |0\rangle\}$ and $\Lambda_- = \{|-1\rangle, |e\rangle, |0\rangle\}$. System Λ_+ has the dark state $|d_+\rangle \propto \cos(\theta)|1\rangle - \frac{1}{\sqrt{2}} e^{i\omega t} \sin(\theta)|0\rangle$ at $\omega \approx \omega_B$, while system Λ_- has the dark state $|d_-\rangle \propto \cos(\theta)|-1\rangle - \frac{1}{\sqrt{2}} e^{i\omega t} \sin(\theta)|0\rangle$ at $\omega \approx -\omega_B$. For $\theta \ll 1$, the dark states $|d_\pm\rangle \approx |\pm 1\rangle$ represent the polarized states perpendicular to the optical axis. The application of magnetic field $B\hat{z}$ separates the CPT resonances of Λ_+ and Λ_- by $2\omega_B$, so that the states $|d_+\rangle$ and $|d_-\rangle$ cannot be simultaneously dark when $\omega_B \gg \Gamma$. Consequently, setting $\omega = \omega_B$ depopulates the Λ_- system while pumping the Λ_+ system towards the transversely oriented dark state $|d_+\rangle$. We conclude that destructive interference of two excitation pathways effectively modifies the absorption selection rules, such that one polarized state (e.g. $|-1\rangle$ for $\omega_B > 0$) absorbs photons, while the opposite state ($|1\rangle$ for $\omega_B > 0$) is transparent.

We associate the two resonances in Fig. 3a with the CPT dark states of Λ_+ at $\omega > 0$ and Λ_- at $\omega < 0$. In the absence of the upper hyperfine level $F_e = 4$, we expect to find distinct resonance peaks at $\pm\omega_B$; it is the presence of $F_e = 4$ that breaks the symmetry between positive and negative ω [$S_z(\omega) \neq -S_z(-\omega)$], generates the small Fano-like features, and shifts the peak from $\omega = \omega_B$. As seen in Fig. 3b, the pumping is most efficient at moderate modulation depths: For $\theta \rightarrow \pi/2$ the dark state is $|d_+\rangle \rightarrow |0\rangle$, with zero net orientation. For $\theta \rightarrow 0$, the dark state is $|d_+\rangle \approx |1\rangle$, but the depopulating rate of $|d_-\rangle$, proportional to $\Gamma \sin^2(\theta)$, is too small compared to the overall depolarization rate γ.

A benefit of the CPT resonant operation is the ability to temporally vary the system state in a controlled, adiabatic manner. To demonstrate this, we monitor the pumping process on resonance [$\omega = \omega_B = 1.5 \ (2\pi)$ kHz], while temporally varying θ over a duration $T = 100$ ms according to $\theta(t) = \arccos\sqrt{t/T}$. The spin state, initially pumped to $|d_+\rangle_{\theta(t=0)} \approx |0\rangle$, adiabatically follows the varying dark state $|d_+\rangle_{\theta(t)}$ to its final value $|d_+\rangle_{\theta(t=T)} \approx |1\rangle$, tracing a spherical-like trajectory as shown in Fig. 2c (experiment) and Fig. 2d (theory). This process is similar to stimulated Raman adiabatic passage[36] and can therefore be used to tailor desired trajectories and final states. Notably, it enables the zeroing of the transverse spin components S_x and S_y at the end of the process, as shown in Fig. 2c, d.

Discussion

It is relatively simple to implement the presented scheme in applications. Polarization modulation can be done using a single photo-elastic modulator (Photoelastic Modulators, www.hindsinstruments.com/products/photoelastic-modulators) or with readily available, on-chip, integrated photonics[37]. Various applications that rely on optical spin manipulation and feature resolved hyperfine spectra could potentially benefit from utilizing the scheme. Here we briefly consider some directions with spin vapors.

First, devices currently employing perpendicular beams in a pump-probe configuration[26–28] could be realized with a simpler, co-propagating arrangement, with the spins oriented transversely to the optical axis. Such arrangement is most beneficial for miniaturized sensors, such as nuclear magnetic resonance (NMR) oscillators[28,29], where the size and complexity depend crucially on the beam's configuration, especially if the light source, manipulation, and detection can be implemented on a single stack over a chip[27]. These sensors are used in various applications as well as in fundamental research, such as search for new physics[29,38]. Particularly for NMR oscillators, the projection of the alkali spin
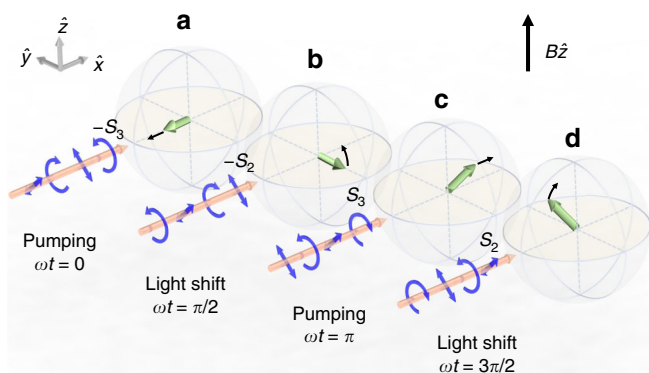

Fig. 4 Transverse pumping mechanism. One period of the transverse pumping mechanism for $\omega = \omega_B$, where the modulation frequency ω is synchronous with the Larmor precession rate ω_B. The spins (green arrows) precess $\omega_B t = \pi/2$ radians between each subplot due to the magnetic field $B\hat{z}$. **a** The spins are optically pumped towards $-\hat{x}$. **b** The spins are tilted towards $+\hat{z}$ due to tensor light shift. **c** The spins are optically pumped towards $+\hat{x}$. **d** The spins are again tilted towards $+\hat{z}$ due to tensor light shift. Black arrows indicate the pumping/tilting directions. The eventual spin orientation is along $+\hat{z}$, perpendicular to the propagation direction of the pumping beam

along the magnetic field will be unmodulated, thus sustaining the spin-exchange optical pumping of the noble gas spins.

Second, any application that is restricted to a single laser direction and requires moderate alkali polarization (tens of percents) can now use our scheme to control and fine-tune the final direction of the pumped spins (longitudinal, transversal, or combination thereof). One example includes remote magnetometry of mesospheric sodium spins[26,39]. Third, transverse pumping may form the basis for an all-optical magnetometer using either alkali-metal atoms or metastable ^{4}He atoms designed for space applications[26,38]. This magnetometer would rely on measuring the resonant response to the modulated light, providing a dead-zone-free operation[32], or on measuring the Faraday rotation of off-resonant probe light, thus reducing the photon shot-noise commonly limiting magnetometers based on electromagnetically induced transparency[40]. Moreover, the polarization-modulated pump generates the $m = 1$ Zeeman coherence[30], implying that these magnetometers could operate in the spin-exchange relaxation-free (SERF) regime[41], where spin-exchange collisions may also assist in repumping the lower hyperfine manifold[42].

Finally, our scheme does not rely on any process particular to vapor physics. It is thus readily applicable to any spin system having a non-degenerate Λ-system with a meta-stable ground manifold, such as those employed in diamond color centers[43,44], rare-earth doped crystals[45], and semiconductor quantum dots[46–48].

In conclusion, we have demonstrated a new optical pumping technique, generating significant spin orientation transversely to the propagation direction of the pump beam. The spins are oriented along the external transverse magnetic field via alternating actions of pumping and tensor light shifts, which are resonant with the Larmor precession. The resonance features, associated with transversely oriented dark states, allow one to control the spin trajectory on the Bloch sphere by varying the modulation parameters. This scheme could be highly suitable for quantum-metrology applications.

Methods

Additional experimental details. We use a 10-mm-diameter, 30-mm-long cylindrical glass cell containing cesium vapor ($I = 7/2$, $S = 1/2$) at room temperature. The cell is paraffin coated and free of buffer gas, exhibiting spin coherence time of 150 ms[30]. We set a constant magnetic field $B\hat{z}$ in the cell using Helmholtz coils and four layers of magnetic shields. For the transverse pumping, we use an 895-nm single-mode pump beam using a free-running distributed Bragg reflector (DBR) diode laser (see optical schematics in Supplementary Fig. 1). We modulate the pump polarization by splitting it with a polarizing beam splitter (PBS) and sending each output arm to an acousto-optic modulator (AOM), operating at 200 MHz. The two beams deflected by the modulators are recombined and mode-matched using a second PBS, resulting with the polarization given in Eq. (1). The pump frequency after passing the modulators is tuned to resonance with the D_1 transition $F_g = 4 \rightarrow F_e = 3$, within the Doppler width. We control the modulation angular frequency ω by setting the relative radio frequencies of the two modulators. We control the modulation depth $\sin(\theta)$ either by rotating the linear polarization using a half-wavelength wave-plate before the first PBS for constant θ (e.g., Figs. 2a, 3c), or by varying the relative RF amplitudes of the two AOMs for a time-varying $\theta(t)$ (e.g., Fig. 2d). We sample the pumping beam before the entrance to the cell and measure the Stokes component S_2 to determine the polarization state of the light. To keep the lower hyperfine manifold $F_g = 3$ empty, we use 1 mW of auxiliary repump beam at 895 nm, using a second free-running DBR laser. The repump is resonant with the $F_g = 3 \rightarrow F_e = 4$ transition, within the Doppler width, and linearly polarized along $\hat{y}$. The pump and repump, both with a diameter of 8 mm, counter-propagate along the $\hat{x}$ axis.

Reconstruction of the spin state on the Bloch sphere. The spin state is reconstructed by evaluating the electronic spin orientations $(2S_x, 2S_y, 2S_z) = \langle \mathbf{F} \rangle / 4$, where $\langle \mathbf{F} \rangle$ is the orientation moment of the total spin operator $\mathbf{F} = \mathbf{I} + \mathbf{S}$. The spin orientations are measured by using balanced polarimetry of two linearly polarized monitor light beams propagating along $\hat{x}$ and $\hat{y}$. The monitor light is 30 GHz blue-detuned from the optical transition $F_g = 4 \rightarrow F_e = 3$. Polarization rotation of far-detuned light is sensitive to spin orientation along the optical axis and insensitive to

higher magnetic moments. At low atomic densities and depopulated $F_g = 3$ hyperfine manifold, the detected Faraday-rotation angles are proportional to the spin orientation along the direction of the beam[2,49]. We calibrate the proportionality constants of each monitor beam by measuring its maximal polarization rotation when the ground state is fully pumped using two circularly polarized beams resonant with the two ground-state hyperfine manifolds. We reconstruct the three spin components by making two consecutive measurements: First, S_x and S_y are measured when $\mathbf{B} = B\hat{z}$. Second, a measurement is conducted with $\mathbf{B} = B\hat{y}$ and θ changed by $\theta \rightarrow \pi/2 - \theta$, keeping the other experimental parameters unchanged. As a result, spin is built along $\hat{y}$ and measured by the $\hat{y}$ monitor. This provides the S_z component of the first configuration. We verify that S_x is unaffected by the change of θ, B, by confirming that the parameter change is appropriate.

Spin dynamics with polarization-modulated light. For small modulation depths $\theta \ll 1$, the dynamics is governed by Bloch-like equations of the vector $\langle \mathbf{F} \rangle = (F_x, F_y, F_z)$ (see Supplementary Note 1 for the general treatment). This dynamics is qualitatively shown in Fig. 4 at four parts of the pumping period: at $\omega t = 0$ [Fig. 4a], at $\omega t = \pi/2$ [Fig. 4b], at $\omega t = \pi$ [Fig. 4c] and at $\omega t = 3\pi/2$ [Fig. 4d]. The spin orientations F_x (along the optical axis) and F_y are subject to

$$\dot{F}_x = -\gamma_\perp F_x - \omega_B F_y - \Gamma \sin(2\theta) \cos(\omega t), \tag{2}$$

$$\dot{F}_y = -\gamma_\perp F_y + \omega_B F_x + \Gamma \sin(2\theta) \sin(\omega t) F_z, \tag{3}$$

which include a transverse decay rate $\gamma_\perp = \gamma + (1 + \cos^2 \theta)\Gamma$ and Larmor precession at the rate ω_B. Here γ denotes a slow ground-state depolarization rate (e.g., due to wall collisions). The third term in Eq. (2) is due to s_3. It describes a temporally modulated optical pumping, which is maximal at $\omega t = 0$ (and at all $\omega t = 2\pi n$ for any integer n) towards $-\hat{x}$ (Fig. 4a) and at $\omega t = \pi$ towards $+\hat{x}$ (Fig. 4c). The pumping of F_x is thus most efficient when the optical modulation is synchronous with the Larmor precession $\omega = \omega_B$. The third term in Eq. (3) is due to the modulated linear polarization component s_2. It describes a tensor light shift, which acts as a magnetic field along $\hat{x}$ that rotates the spins in the yz plane at a modulated rate $\Gamma \sin(2\theta) \sin(\omega t)$. The orientation F_z along the magnetic field, which we aim to generate, is subject to

$$\dot{F}_z = -\gamma_\parallel F_z - \Gamma \sin(2\theta) \left[\sin(\omega t) F_y - \cos(\omega t) \{F_z, F_x\} \right], \tag{4}$$

where the first term is a longitudinal decay at a rate $\gamma_\parallel = \gamma + 2\Gamma \sin^2 \theta$, the second term is again light shift due to s_2, and the third term is an alignment-induced shift. The temporal modulation $\sin(\omega t)$ of the light shift is a key ingredient in pumping $\mathbf{F}$ towards $+\hat{z}$, as it breaks the symmetry between the $\pm \hat{z}$ directions: The sign of the light shift changes together with the sign of F_y, thus acting as an alternating magnetic field that always tilts the spins -towards $+\hat{z}$, with maximal tilting rate obtained at $\omega t = \pi/2$ (Fig. 4b) and $\omega t = 3\pi/2$ (Fig. 4d). The tensor term $\{F_z, F_x\} \equiv \langle \{\mathbf{F}\hat{z}, \mathbf{F}\hat{x}\} \rangle$, resonant at ω_B, contributes similar spin buildup in amplitude, but with a $\pi/2$ delay (see Supplementary Note 1). Contribution of other tensor terms resonant at $2\omega_B$ is negligible for $\omega \approx \omega_B \gg \Gamma$. For $\omega = \omega_B$, both the synchronous pumping and the light shift are most efficient, driving the precessing spins away from the xy plane, transversely to the optical axis. For large magnetic fields and strong control beam $\omega_B \gg \Gamma \gg \Gamma \sin^2 \theta, \gamma$, the steady-state polarization on resonance ($\omega = \omega_B$) is given by

$$F_z = \frac{\Gamma \sin^2 \theta}{\Gamma \sin^2 \theta + \gamma},$$

where $\Gamma \sin^2 \theta$ can be interpreted as the effective optical pumping rate for depopulating the bright state $|-1\rangle$ (see derivation in Supplementary Note 2). The transverse spin components are then given by $F_x = \tan \theta \cos (\Delta t + \pi)(1 + F_z)/2$, and $F_y = \tan \theta \sin(\Delta t)(1 + F_z)/2$, where $\Delta = \omega - \omega_B$ denotes the frequency mismatch from resonance. We thus conclude that high polarization along the magnetic field and transverse to the optical axis is achievable for $I = 1/2$ spins.

Data availability

The data that support the findings of this study are available from the corresponding author on reasonable request.

References

1. Happer, W. Optical pumping. *Rev. Mod. Phys.* **44**, 169 (1972).
2. Happer, W., Jau, Y.-Y. & Walker, T. G. *Optically Pumped Atoms* (Wiley, New York, 2009).
3. Auzinsh, M., Budker, D. & Rochester, S. M. *Optically Polarized Atoms: Understanding Light-Atom Interactions*. 1st edn (Oxford University Press, Oxford, 2010).

4. Budker, D. & Romalis, M. V. Optical magnetometry. *Nat. Phys.* **3**, 227 (2007).
5. Kominis, I. K., Kornack, T. W., Allred, J. C. & Romalis, M. V. *Nature* **422**, 596–599 (2003).
6. Kitching, J., Knappe, S. & Donley, E. A. Atomic sensors – a review. *IEEE Sens. J.* **11**, 1749 (2011).
7. Horsley, A., Du, G. X. & Treutlein, P. Widefield microwave imaging in alkali vapor cells with sub-100 mm resolution. *New J. Phys.* **17**, 112002 (2015).
8. Hammerer, K., Sørensen, A. S. & Polzik, E. S. Quantum interface between light and atomic ensembles. *Rev. Mod. Phys.* **82**, 1041–1093 (2010).
9. Møller, C. B. et al. Quantum back-action-evading measurement of motion in a negative mass reference frame. *Nature* **547**, 191 (2017).
10. Novikova, I., Walsworth, R. & Xiao, Y. Electromagnetically induced transparency-based slow and stored light in warm atoms. *Laser Photon. Rev.* **6**, 333–353 (2012).
11. Walker, T. G. & Happer, W. Spin-exchange optical pumping of noble-gas nuclei. *Rev. Mod. Phys.* **69**, 629 (1997).
12. Appelt, S. et al. Theory of spin-exchange optical pumping of ^{3}He and ^{129}Xe. *Phys. Rev. A* **58**, 1412 (1998).
13. Chupp, T. & Swanson, S. Medical imaging with laser-polarized noble gases. *Adv. Mol. Opt. Phys.* **45**, 41 (2001).
14. Kuchler, F. et al. A new search for the atomic EDM of ^{129}Xe at FRM-II. *Hyperfine Interact.* **237**, 95 (2016).
15. Vasilakis, G., Brown, J. M., Kornack, T. W. & Romalis, M. V. Limits on new long range nuclear spin-dependent forces set with a K−^{3}He comagnetometer. *Phys. Rev. Lett.* **103**, 261801 (2009).
16. Romalis, M. V. Hybrid optical pumping of optically dense alkali-metal vapor without quenching gas. *Phys. Rev. Lett.* **105**, 243001 (2010).
17. Kornack, T. W. *A Test of CPT and Lorentz Symmetry Using a K-3He Co-magnetometer.* Ph.D. thesis (Princeton University, Princeton, 2005).
18. Muschik, C. A., Polzik, E. S. & Cirac, J. I. Dissipatively driven entanglement of two macroscopic atomic ensembles. *Phys. Rev. A* **83**, 052312 (2011).
19. Fescenko, I., Knowles, P., Weis, A. & Breschi, E. A Bell-Bloom experiment with polarization-modulated light of arbitrary duty cycle. *Opt. Express* **21**, 15121 (2013).
20. Seltzer, S. J., Meares, P. J. & Romalis, M. V. Synchronous optical pumping of quantum revival beats for atomic magnetometry. *Phys. Rev. A* **75**, 051407(R) (2007).
21. Klepel, H. & Suter, D. Transverse optical pumping with polarization-modulated light. *Opt. Commun.* **90**, 46 (1992).
22. Chalupczak, W. et al. Enhancement of optically pumped spin orientation via spin-exchange collisions at low vapor density. *Phys. Rev. A* **85**, 043402 (2012).
23. Chalupczak, W. & Josephs-Franks, P. Alkali-metal spin maser. *Phys. Rev. Lett.* **115**, 033004 (2015).
24. Budker, D., Kimball, D. F., Rochester, S. M. & Yashchuk, V. V. Nonlinear magneto-optical rotation via alignment-to-orientation conversion. *Phys. Rev. Lett.* **85**, 2088 (2000).
25. Budker, D. et al. Resonant nonlinear magneto-optical effects in atoms. *Rev. Mod. Phys.* **74**, 1153 (2002).
26. Budker, D. & Jackson Kimball, D. F. *Optical Magnetometry* (Cambridge University Press, New York, 2013).
27. Kitching, J. et al. Microfabricated atomic magnetometers and applications. in *Frequency Control Symposium, IEEE International*, 789–794 (IEEE, 2008).
28. Walker, T. G. & Larsen, M. Spin-exchange-pumped NMR gyros. *Adv. Mol. Opt. Phys.* **65**, 373–401 (2016).
29. Bulatowicz, M. et al. Laboratory search for a long-range *T*-Odd, *P*-Odd interaction from axionlike particles using dual-species nuclear magnetic resonance with polarized ^{129}Xe and ^{131}Xe gas. *Phys. Rev. Lett.* **111**, 102001 (2013).
30. Katz, O. & Firstenberg, O. Light storage for one second in room-temperature alkali vapor. *Nat. Commun.* **9**, 2074 (2018).
31. Martin, C., Walker, T., Anderson, L. W. & Swenson, D. R. Laser optical pumping of potassium in a high magnetic field using linearly polarized light. *Nucl. Instrum. Methods Phys. Res. Sect. A* **335**, 233 (1993).
32. Ben-Kish, A. & Romalis, M. V. Phys. dead-zone-free atomic magnetometry with simultaneous excitation of orientation and alignment resonances. *Rev. Lett.* **105**, 193601 (2010).
33. Novikova, I., Mikhailov, E. E. & Xiao, Y. Excess optical quantum noise in atomic sensors. *Phys. Rev. A* **91**, 051804(R) (2015).
34. Cohen-Tannoudji, C. & Dupont-Roc, J. Experimental study of Zeeman light shifts in weak magnetic fields. *Phys. Rev. A* **5**, 968 (1972).
35. Fleischhauer, M., Imamoglu, A. & Marangos, J. P. Electromagnetically induced transparency: optics in coherent media. *Rev. Mod. Phys.* **77**, 633 (2005).
36. Vitanov, N. V., Rangelov, A. A., Shore, B. W. & Bergmann, K. Stimulated Raman adiabatic passage in physics, chemistry, and beyond. *Rev. Mod. Phys.* **89**, 015006 (2017).
37. Sarmiento-Merenguel, J. D. et al. Demonstration of integrated polarization control with a 40 dB range in extinction ratio. *Optica* **2**, 1019–1023 (2015).
38. Patton, B., Zhivun, E., Hovde, D. C. & Budker, D. All-optical vector atomic magnetometer. *Phys. Rev. Lett.* **113**, 013001 (2014).
39. Higbie, J. M. et al. Magnetometry with mesospheric sodium. *Proc. Natl Acad. Sci. USA* **108**, 3522 (2011).
40. Fleischhauer, M., Matsko, A. B. & Scully, M. O. Quantum limit of optical magnetometry in the presence of ac Stark shifts. *Phys. Rev. A* **62**, 013808 (2000).
41. Katz, O. et al. Nonlinear elimination of spin-exchange relaxation of high magnetic moments. *Phys. Rev. Lett.* **110**, 263004 (2013).
42. Chalupczak, W., Josephs-Franks, P., Patton, B. & Pustelny, S. Spin-exchange narrowing of the atomic ground-state resonances. *Phys. Rev. A* **90**, 042509 (2014).
43. Yale, C. G. et al. All-optical control of a solid-state spin using coherent dark states. *Proc. Natl Acad. Sci. USA* **110**, 7595 (2013).
44. Zhou, B. B. et al. Holonomic quantum control by coherent optical excitation in diamond. *Phys. Rev. Lett.* **119**, 140503 (2017).
45. Schraft, D., Hain, M., Lorenz, N. & Halfmann, T. Stopped light at high storage efficiency in a Pr^{3+}:Y$_2$SiO$_5$ crystal. *Phys. Rev. Lett.* **116**, 073602 (2016).
46. Weiss, K. M. et al. Coherent two-electron spin qubits in an optically active pair of coupled InGaAs quantum dots. *Phys. Rev. Lett.* **109**, 107401 (2012).
47. Houel, J. et al. High resolution coherent population trapping on a single hole spin in a semiconductor quantum dot. *Phys. Rev. Lett.* **112**, 107401 (2014).
48. Weinzetl, C. et al. Coherent control and wave mixing in an ensemble of silicon-vacancy centers in diamond. *Phys. Rev. Lett.* **122**, 063601 (2019).
49. Katz, O., Peleg, O. & Firstenberg, O. Coherent coupling of alkali atoms by random collisions. *Phys. Rev. Lett.* **115**, 113003 (2015).

Acknowledgements

Author contributions

O.K. conducted the experiment and analyzed the data. O.F. and O.K. designed the experiment, performed the theoretical analyses, and wrote the paper.

Additional information